Impact of material characteristics on the self-healing kinetic of cementitious materials

Kelly Olivier, Aveline Darquennes, Farid Benboudjema, Richard Gagné

ENS CACHAN, FRANCE MAY 11th & 12th, 2015 CIGOS - PARIS 2015
International Conference
INNOVATIONS IN CONSTRUCTION

Impact of material characteristics on the self-healing kinetic of cementitious materials

Kelly OLIVIER

ENS Cachan / LMT-CNRS UMR8535 / UPMC / PRES-UniverSud Paris (kelly.olivier@ens-cachan.fr)

Centre de recherche sur les infrastructures en béton (CRIB), Université de Sherbrooke, Québec, Canada

Aveline DARQUENNES

ENS Cachan / LMT-CNRS UMR8535 / UPMC / PRES-UniverSud Paris (aveline.darquennes@ens-cachan.fr)

Farid BENBOUDJEMA

ENS Cachan / LMT-CNRS UMR8535 / UPMC / PRES-UniverSud Paris (farid.benboudjema@dgc.ens-cachan.fr)

Richard GAGNÉ

Centre de recherche sur les infrastructures en béton (CRIB), Université de Sherbrooke, Québec, Canada (richard.gagne@usherbrooke.ca)

Abstract (Maximum 250 words):

Cement is one of the most useful materials in the world. Concrete made with this material presents many advantages such as workability and durability. However, cement production releases a lot of CO_2. To limit this effect, cement can be replaced by mineral additions. Ground granulated blast-furnace slag (GGBFS), an industrial waste of iron manufacturing, can be recycled as a cementitious material. Moreover, it improves some properties of concrete such as workability, sulphate resistance, etc. However, concrete made with blast-furnace slag presents cracking risk under restraint conditions and can affect the durability by allowing the penetration of aggressive agents.
Previous researches have proved that self-healing of cracks can limit this problem. To understand the role of GGBFS on self-healing and the impact of material characteristics on the kinetics of the phenomenon, three compositions of mortar characterized by several GGBFS contents were tested Mortar specimens were cracked at 7 days after casting and stored in water at 23°C. The volume evolution of self-healing products was monitored by X-ray tomography. The hydration degree of mortars was computed from TGA measurements. After one year, SEM with EDS was performed to identify the products formed inside the crack.
Results showed that hydration products were formed by the hydration of anhydrous particles on the crack surface. Mortar made with GGBFS presented the best self-healing potential. These results were explained by the material characteristics but also by the evolution of its hydration degree.

Keywords (5): Self-healing, blast-furnace slag, cement, SEM, EDS, X-ray tomography

Main subthemes (Tick one item):

☐ Modeling of structures (AMS)

X Materials for construction (MFC)

 Innovative design and methods in construction (IDM)

 Geotechnics for environment and energy (GEE)

1. Introduction

Concrete made with ground granulated blast-furnace slag (GGBFS) cement is often used in civil-engineering structures. It offers many advantages such as reclamation of an industrial waste, decreased CO_2 emissions produced during the clinkerization process in cement manufacturing, and several enhanced material properties, such as workability and long-term compressive strength. It is also appropriate for structures in aggressive environments (farm silos, water-treatment plants, mining) because of its high resistance to sulfate attack and chloride diffusion (Darquennes 2011).

Nevertheless, some civil-engineering structures made with GGBFS cement present cracking at early age due to restrained shrinkage (Darquennes 2012, Briffaut 2012). This cracking can lead to an increased risk of penetration by aggressive agents such as CO_2 and chloride.

Structures made with GGBFS cement, however, have evidenced some self-healing of these cracks. This phenomenon seems to be related to the hydration of anhydrous particles at early age (GGBFS, clinker) (Hearn 1998, Ter Heide 2005) and/or calcite formation due to portlandite carbonation on the long term (Argouges 2011). New hydrates formed in the cracks can partially or completely fill the crack volume. It is not yet clear how GGBFS is involved in the self-healing phenomenon. Indeed, the few available experimental results (Qian 2009, Van Tittelboom 2012) are sometimes contradictory. For example, Van Tittelboom (2012) indicated that the addition of GGBFS positively influenced self-healing, whereas Qian (2009) found the opposite.

In this study, X-ray computed tomography (X-ray CT) was used to monitor self-healing evolution and to determine the effect of GGBFS addition on a macro-scale. X-ray CT offers several advantages over conventional analysis methods such as permeability tests, mechanical tests and scanning electronic microscopy (SEM) (Jacobsen 1995, Granger 2007, Van Tittelboom 2011). For example, it is nondestructive and does not require pretreatment of samples. Moreover, X-ray CT can assess the spatial and temporal evolutions of self-healing on the same sample throughout an experimental campaign and yield a 3-D distribution of the healing products in the sample volume (Poinard 2012, Landis 2013).

The X-ray CT analysis was completed by SEM (scanning electron microscopy) and EDS (energy dispersion spectroscopy) to identify the microstructure of self-healing products. A thermogravimetric analysis was also used to quantify the evolution of boundary water and the portlandite content of the different formulations.

2. Materials and methods

2.1. Materials

The three mortar compositions were (1) a mortar with a binder containing 100% Portland cement (CEMI 52.5 N CP2 NF), (2) a mortar with 50% Portland cement (CEMI 52.5 N CP2 NF) and 50% GGBFS and (3) a mortar with 100% blended cement (CEMIII/A) composed with 62% GGBFS and 32% clinker (same clinker as CEMI 52.5 N CP2 NF used for others formulations) (Table 1. Mortar compositions.). Their water/binder (W/B) ratios were equal to 0.50, 0.52 and 0.50; their binder contents were 563, 539 and 563 kg/m^3, respectively. The cement paste content, a parameter affecting strongly the shrinkage amplitude, was kept constant for both mixes and the same normalized siliceous sand was used (EN 196-1).

Table 1. Mortar compositions.

	Cement [kg/m^3]	Water [kg/m^3]	Sand [kg/m^3]	GGBFS [kg/m^3]
CEMI	563	281	1409	/
CEMI+S	281	281	1409	258
CEMIII/A	563	281	1409	/

X-ray diffraction and X-ray fluorescence (Table 2) were performed to characterize the cementitious materials. X-ray diffraction revealed that the Portland cement was principally composed of C_3S, C_2S, C_3A, and C_4AF. The GGBFS showed amorphous behavior with some crystalline peaks of akermanite, melilite, and merwinite. The CEMIII/A was principally composed of C_3S, C_2S, C_3A, and C_4AF with an incurved spectrum as GGBFS (bump between [20-40°]). The CEMI was mainly composed of CaO (64.85%). The slag contained a smaller proportion of CaO (43.21%) than the CEMI, but greater amounts of SiO_2 (33.08%), Al_2O_3 (9.50%), and MgO (5.77%). The composition of CEMIII/A is between these two materials with 51.85% of CaO, 27.95% of SiO_2, 7.76% of Al_2O_3 and 4.06% of MgO. The hydraulic factor ($Hydraulic\ factor = \frac{CaO+MgO+Al_2O_3}{SiO_2}$ (Eq. 1)) was up to 1 for the GGBFS (1.76), indicating a good reactivity. Table 3 presents the results of laser particle-size distribution (PSD) testing. They reveal that the slag is finer than the CEMI and CEMIII/A with 48.68% of its particles below 10 µm compared to 36.37% for the CEMI and 40.91% CEMIII/A.

$$Hydraulic\ factor = \frac{CaO+MgO+Al_2O_3}{SiO_2} \quad \textbf{(Eq. 1)}$$

Table 2. Chemical compositions of the CEMI, CEMI+S and CEMIII/A.

Oxides [%]	CEMI	GGBFS	CEMIII/A
CaO	64.85	43.21	51.85
SiO_2	18.60	33.08	27.95
Al_2O_3	4.92	9.50	7.76
MgO	1.15	5.77	4.06

Table 3. Particle-size distribution of the CEMI, CEMI+S and CEMIII/A.

% <	CEMI	CEMI+S	CEMIII/A
1 µm	4.31	4.36	3.97
10 µm	36.37	48.68	40.91
100 µm	99.94	100.00	100.00

2.2. Methods

2.2.1. X-ray tomography

Specimen dimensions play a significant role in X-ray CT picture resolution. To achieve a reasonable voxel size (20 µm), cylindrical specimens with a 4 cm diameter (height h = 10 cm) were tested. After mixing, the specimen were kept in a room at 23°C ± 1°C and 45% ± 5% of relative humidity (RH). The molds were removed after 2 days and the specimens were stored underwater at 23°C ± 1°C. At 6 days, they were confined with a two-component resin reinforced with glass fibers. At 7 days, the specimens were cracked along the diameter with a splitting-tensile test. Then, the samples were sawn into 2 cm thick disks and scanned using X-ray CT to determine their initial state. The samples were then stored in tap water at 23°C ± 1°C in individual containers. The specimens were regularly analyzed with tomography during a month to monitor self-healing.
During the tomography, a sample was placed on a rotating support between the X-ray tube and detector. Three scans were performed for each table position (600 positions). The test parameters of position number for one test, high-voltage, target power, and frames per second were 600, 160 kV, 5.5 W, and 0.4, respectively. Afterwards, a 3-D image of the specimen was reconstructed (using efX-CT software). For these 3-D images, the material volumes characterized by lower density such as air, show a darker grey level. Artefacts around the specimen can be seen after reconstruction. To limit the effect of these artefacts during the analysis, a sub-volume was isolated inside the specimen (Figure 1. Location of sub-volume).

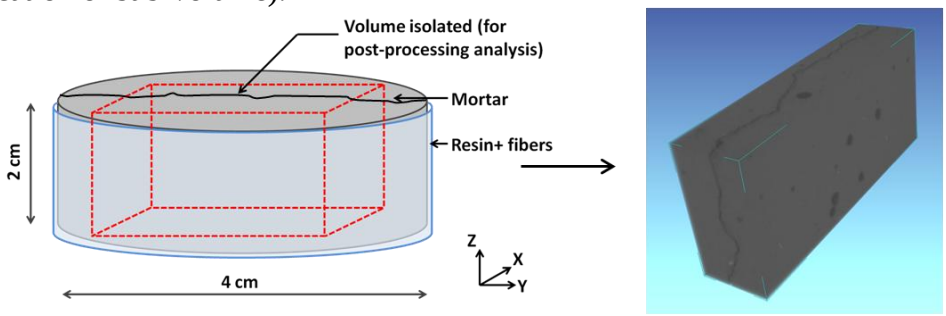

Figure 1. Location of sub-volume

To assess the evolution of crack volume, the 3-D X-ray tomography images (1300 x 300 x 600 voxels, with 256 gray levels) underwent a post-processing. Firstly, the 3-D image was transformed into a set of pictures along the Z-axis containing 600 pictures with a size of 1300 by 300 pixels.
A segmentation algorithm and a connected-component analysis algorithm were applied in each picture to determine the gray-level threshold corresponding to the cracked volume (Landis, 2013).
In this study, one specimen was tested for the CEMI and two for the CEMI+S and three for CEMIII/A to estimate the repeatability.

2.2.2. SEM-EDS

One year after the X-ray CT campaign, scanning electron microscopy (SEM) with energy dispersive X-ray spectroscopy (EDS) analysis was performed on specimens to determine new products formed in the crack. The specimens were stored in tap water.

2.2.3. Thermogravimetric analysis

Thermogravimetric analysis (TGA) was performed on mortar specimens to determine their hydration kinetics. The weight-loss evolution of a specimen was monitored between 50°C and 1,000°C with a heat rate of 10°C/min in an argon environment. The samples were tested at 2, 3, 7, 14, 28, and 90 days. Before the test, they were stored in tap water in a room controlled at 23°C. A few minutes before the test, 2 g of mortar was ground and about 60 mg placed in an alumina

crucible. An empty crucible was used as reference and placed close to the sample. Three tests were performed for each measurement.

The boundary water was quantified by the mass-loss difference from 105°C to 1,000°C and from 600°C to 880°C (decarbonation of $CaCO_3$). The temperature of 105°C corresponds to free-water evaporation. The boundary water ($w(t) = \frac{|\Delta m_{105\rightarrow1000°C}(t)| - |\Delta m_{600\rightarrow880°C}(t)| - m_{sand} * LOI_{sand} - \sum m_k LOI_k}{m_b + m_{sand} * LOI_{sand}}$ (Eq. 2) is expressed as cement mass (Popic 2010):

$$w(t) = \frac{|\Delta m_{105\rightarrow1000°C}(t)| - |\Delta m_{600\rightarrow880°C}(t)| - m_{sand} * LOI_{sand} - \sum m_k LOI_k}{m_b + m_{sand} * LOI_{sand}} \quad \textbf{(Eq. 2)}$$

where w(t) is the boundary water (g/g_{binder}) at time t, $\Delta m_{i\rightarrow j}$ is the mass loss between temperatures i to j (g), m_{sand} is the sand mass in the sample (g), LOI_{sand} is the sand's loss on ignition (%), m_k is the cement or slag mass (g), LOI_k is the loss on ignition of the cement or slag (%), and m_b is the binder mass in the sample (g).

Moreover, it was necessary to determine the ultimate boundary water w_∞. To compute w_∞, we used the experimental approach proposed by Bentz (1995). This consists in mixing a cement paste (water/binder ratio equal to 3.0) with steel balls in a hermetic bottle during 56 days. Then, TGA was performed to determine the boundary water necessary to hydrate whole grains of cement and slag. Before the test, the cement paste was dried for 1 h at 80°C to produce a dry material for the TGA.

Finally, the portlandite content was determined to assess the evolution of slag reaction. The portlandite content is computed with ($Portlandite\ content = \frac{|\Delta m_{400\rightarrow600°C}(t)|}{m_b + m_{sand} LOI_{sand}} * \frac{M_{Ca(OH)2}}{M_{H2O}}$ (Eq. 3):

$$Portlandite\ content = \frac{|\Delta m_{400\rightarrow600°C}(t)|}{m_b + m_{sand} LOI_{sand}} * \frac{M_{Ca(OH)2}}{M_{H2O}} \quad \textbf{(Eq. 3)}$$

where $\Delta m_{400\rightarrow600°C}$ is the mass loss from 400°C to 600°C (g), m_b is the binder mass (g), m_{sand} is the sand mass in the sample (g), LOI_{sand} is the sand's loss on ignition (%) and $M_{Ca(OH)2}$ and M_{H2O} are, respectively, the molar mass of portlandite and water ($g.mol^{-1}$).

3. Results

3.1. Volume evolution of self-healing products

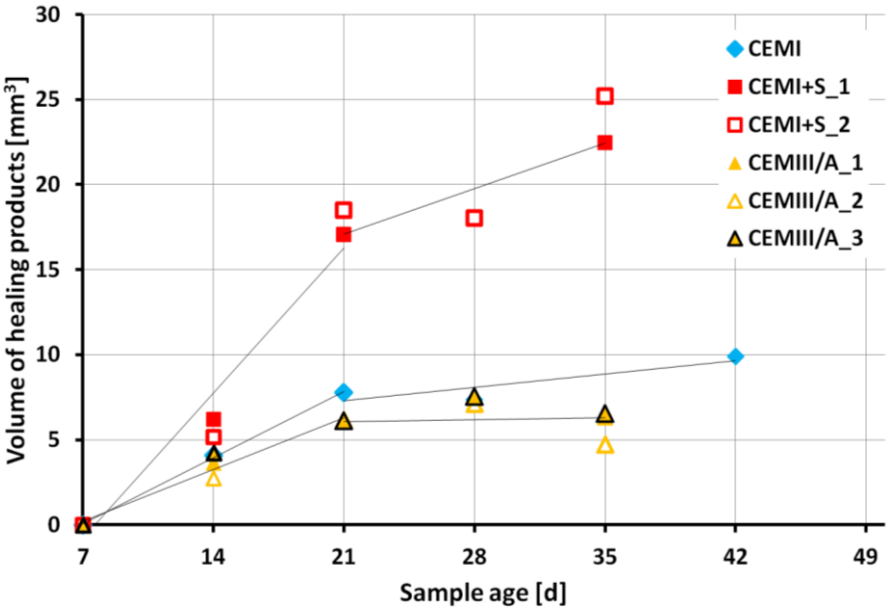

Figure 2. Volume evolution of healing products

Figure 2. Volume evolution of healing products shows that the volume of healing products increased for all the mortar compositions with the duration of water storage. The change is faster during the first 15 days after cracking. Subsequently, healing-product formation slowed (the crack volume continued to decrease but at a slower rate). This is in agreement with Argouges (2009), who showed that the kinetics of self-healing is characterized by two stages. Argouges followed self-healing after one and three month. In that case, self-healing is faster during the first month after cracking.

Two CEMI+S mortars and three CEMIII/A mortars were tested to check test repeatability. All specimens of CEMIII/A show a same self-healing behavior with standard deviations between 0.02 and 0.8 mm^3. Both CEMI+S samples have the same tendency: the kinetic of the formation of self-healing products decreases after about 21 days (age of sample). Indeed, it is equal to 1.22 $mm^3.d^{-1}$ for CEMI+S_1 and 1.32 $mm^3.d^{-1}$ for CEMI+S_2 before 21 days and to 0.38 $mm^3.d^{-1}$ for slag CEMI+S_1 and 0.48 $mm^3.d^{-1}$ for CEMI+S_2 after this time. In both cases, the CEMI+S mortar presents greater self-healing than the CEMI and the CEMIII/A mortars. At 7 and 14 days after cracking, the average volume of the self-healed products are, respectively, (1) 4.08 mm^3 and 7.77 mm^3 for the CEMI mortar, (2) 5.66 mm^3 ± 0.53 mm^3, 17.78 mm^3 ± 0.71 mm^3 for the CEMI+S mortar and (3) 3.54 mm^3 ± 0.76 mm^3, 6.10 mm^3 ± 0.04 mm^3 for the CEMIII/A mortar. Thus, the formation of new products is higher for the CEMI+S mortar and lower for the CEMIII/A than for the CEMI. Results in Figure 2. Volume evolution of healing products show that the CEMI+S mortar is characterized by a faster initial self-healing evolution rate than the CEMI mortar and CEMIII/A. The self-healing evolution rate of the CEMI+S is approximately 2 times faster for CEMI and 3 time faster for CEMIII/A. The healed volume is 9.88 mm^3 at 42 days for the CEMI mortar, 22.45 mm^3 and 25.20 mm^3 at 35 days respectively for the CEMI+S _1 and the CEM+S_2 and respectively 6.31 mm^3, 4.74 mm^3 and 6.53 mm^3 at 35 days for CEMIII/A_1, CEMIII/A_2 and CEMIII/A_3.

Two factors can account for this and are discussed below: initial crack size and degree of hydration.

3.1.1. Initial Crack Size

The self-healing kinetics depends on the crack width (Gagné, 2012). Small cracks tend to self-heal more completely at long term because of the smaller initial volume having be filled (Gagné 2012, Edvardsen 1999). The initial crack opening in the CEMI mortar was 113 µm, while the crack opening in the CEMI+S_1 mortar was 71 µm and 115 µm for CEMI+S_2. For the CEMIII/A, the three samples (CEMIII/A_1, CEMIII/A_2, CEMIII/A_3) had respectively an initial crack opening: 159 µm, 289 µm and 214 µm. Even if these initial crack opening are different, the volume evolution of self-healing products are closed for the three CEMIII/A samples and for the two CEMI+S samples. Therefore, the cracking-size effect does not responsible for the different behaviour between slag and control mortar.

3.1.2. Evolution of Degree of Hydration

Binders with GGBFS have a slower evolution rate of hydration at early age according to Darquennes (2013). This leads to a greater amount of anhydrous products at the cracking age (7 days) and, therefore, a higher self-healing potential. From thermogravimetric analysis, the degree of hydration for the two formulations is calculated using the boundary water content $\alpha(t) = \frac{w(t)}{w_\infty} * \alpha_u$ (Eq. 4).

$$\alpha(t) = \frac{w(t)}{w_\infty} * \alpha_u \quad \textbf{(Eq. 4)}$$

Two parameters need to be determined in this relation:
- The final boundary water w_∞. Based on the experimental approach developed by Bentz (1995), the values of the final boundary water w_∞ for the CEMI, CEMI+S and CEMIII/A mortars are 22.90 g/g_{binder}, 20.45 g/g_{binder} and 21.69 g/g_{binder}, respectively and are in agreement with Popic (2010).
- The ultimate hydration degree α_u. In the case of cementitious materials with mineral additions, Schindler (2005) suggested a relation providing the ultimate hydration value $\alpha_u = \frac{1.031 * \frac{W}{C}}{0.194 + \frac{W}{C}} + 0.50 * p_{FA} + 0.30 * p_{slag}$ (Eq. 5):

$$\alpha_u = \frac{1.031 * \frac{W}{C}}{0.194 + \frac{W}{C}} + 0.50 * p_{FA} + 0.30 * p_{slag} \quad \textbf{(Eq. 5)}$$

where W/C is the water–cement ratio, p_{FA} and p_{slag} are the fly ash and the slag in percentages. The α_u for CEMI, CEMI+S and CEMIIIA/ are, respectively, 0.74, 0.90 and 0.93.

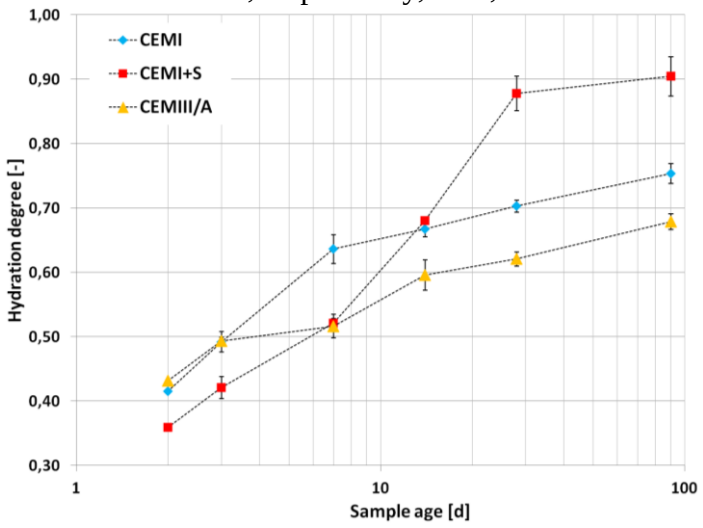

Figure 3. Hydration degree

Figure 3**. Hydration degree** and Figure 4**. Portlandite content** present the averages degree of hydration and portlandite content over time.

During 90 days, the portlandite evolution of CEMI, CEMI+S and CEMIII/A are respectively: 76%, 40%, 16% with final values equal to: $10.83.10^{-2}$ g/g_{binder}, $5.76.10^{-2}$ g/g_{binder} and $3.92.10^{-2}$ g/g_{binder}. The slower evolution of GGBFS mortars is explained by (1) the smaller amount of clinker in the GGBFS mortars, and (2) the consumption of portlandite for reaction of GGBFS particles.

Before the two first weeks, the lower hydration of CEMI+S (14% lower than CEMI and CEMIII/A at 7 days) and higher hydration of CEMIII/A can be explained respectively by the GGBFS's latent hydration properties and the material fineness. The GGBFS's latent hydration property is related to two phenomena (Moranville 2004, Taylor 1997): (1) initiating GGBFS dissolution requires high pH in the interstitial water, which is directly related to its alkali content (e.g., Ca^{2+}); and (2) the GGBFS reaction requires portlandite (see previously, Figure 4**. Portlandite content**) to create supplementary C-S-H. After this time, hydration degree of CEMI+S increases and is 20% upper than CEMI and 31% upper than CEMIII/A.

The portlandite content of CEMIII/A is lower than the two others formulations during the test. However, before 7 days, its hydration degree is closed to that of the CEMI. Even if CEMIII/A mortar is composed by 62% of slag, its good reactivity at 2 and 3 days can be explained by its high fineness (Table 2).

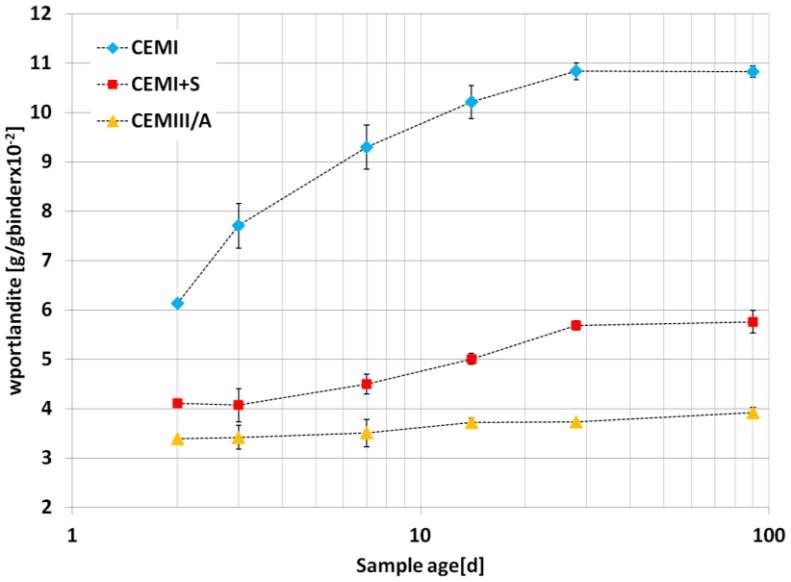

Figure 4. Portlandite content

Subsequent hydration continued slowly, achieving a constant value near the ultimate degree of hydration for CEMI and CEMI+S (0.75 for the CEMI mortar, 0.90 for the CEMI+S mortar at 90 days). At the opposite, the hydration degree of CEMIII/A at 90 days (0.68) was not close to the ultimate hydration degree. The results reveal an average variability of 0.015 (degree-of-hydration value).

These results confirm the slower rate of hydration and, therefore, the greater number of anhydrous particles in the CEMI+S at early age. The different behaviour of CEMIII/A can be explained by its higher initial reactivity. The fast hydration at 2 and 3 days can form a high quantity of hydration products around anhydrous particles and slow down their hydration.

3.1.3. Microstructure of Self-Healing Products

Figure 5. Self-healing products in CEMI, Figure 6. Self-healing products in CEMI+S and Figure 7. Self-healing products in CEMIII/A illustrate self-healed cracks in the CEMI, CEMI+S and CEMIII/A mortars. While sawing may have slightly damaged the new products, the bridging between the two crack faces are clearly visible. EDS analysis of specimens reveal that the new products are C-S-H. In the case of the CEMI+S and CEMIII/A mortars, the C/S ratio is lower than in the CEMI mortar. Moreover, EDS analysis of the new hydrated products in the slag mortars show the presence of alumina and iron ions from GGBFS. These differences between C-S-H in the slag and CEMI mortars have been reported in the literature (Moranville 2004, Taylor 1997). The C-S-H formation confirms that the self-healing of early-age cracks corresponds to ongoing hydration.

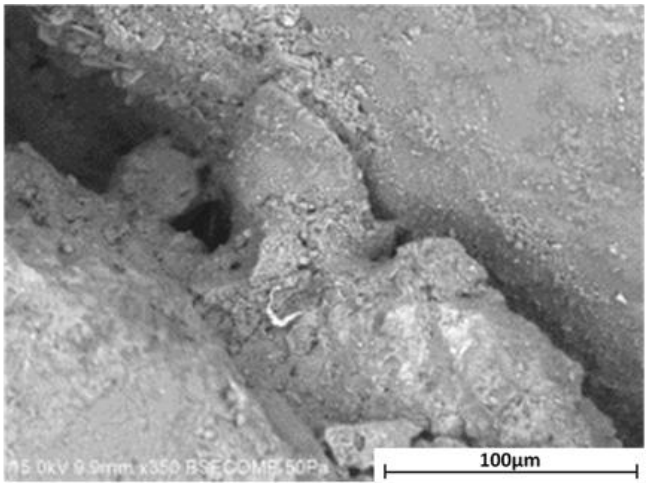

Figure 5. Self-healing products in CEMI

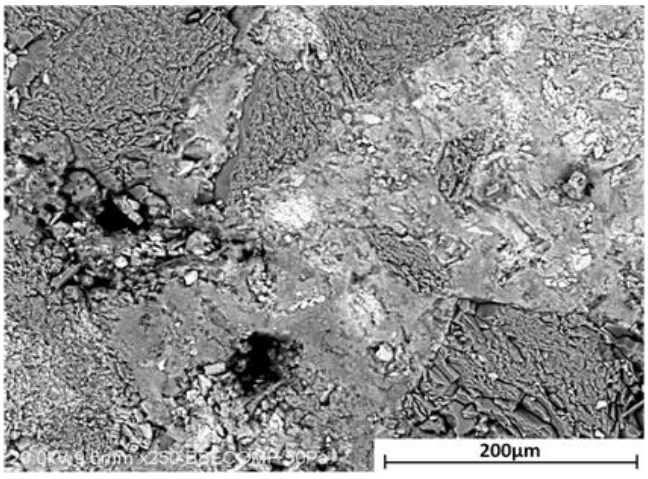

Figure 6. Self-healing products in CEMI+S

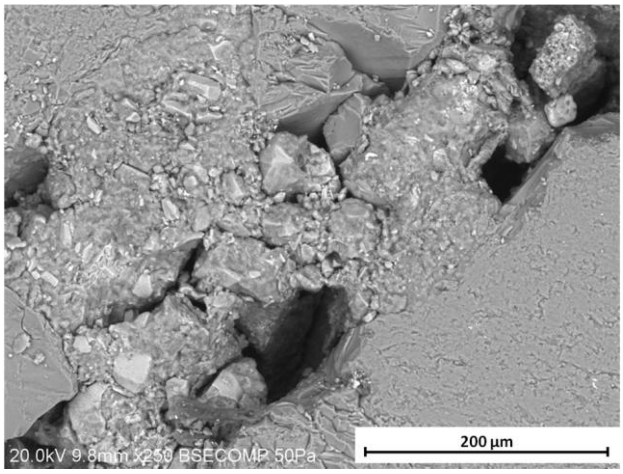

Figure 7. Self-healing products in CEMIII/A

4. Conclusions

This study examined the self-healing phenomenon in cementitious materials with high GGBFS content by conventional (SEM) and original (X-ray CT) means, yielding more information about the self-healing phenomenon and underlining the benefit of GGBFS addition in accelerating this phenomenon. The main results of this study are summarized below.

- X-ray tomography is an effective technique for observing the self-healing phenomenon in 3-D as well as to assess crack evolution and the formation of healing products. The advantage of X-ray CT is that the technique is nondestructive and it provides 3D information on the formation of the self-healing products in the crack.
- For a low hydration degree at the cracking day, mixes with ground granulated blast-furnace slag have a significant capacity for self-healing due to its latent hydraulic and pouzzolanic properties, leading to a significant quantity of unhydrated GGBFS particles at early age.
- Under favorable storage conditions (underwater), at early age and when crack size is limited, the self-healing phenomenon improves material durability for all the studied materials.
- C-S-H was the main self-healing product for all the studied mortar compositions. The early age cracking and the storage underwater (without CO_2) justified these products formations.

Acknowledgment

This work has benefited from the support of the French "Agence Nationale de la Recherche", through the "Investissements d'avenir" program under the reference "ANR-10-EQPX-37 MATMECA.

References

Darquennes, A., Staquet, S., Espion, B., 2011, Behaviour of slag cement concrete under restraint conditions, *European Journal of Environmental and Civil Engineering*, 15/7, 1017-1029.

Darquennes, A., Rozière, E., Khokhar, M., I., A., Turcry, P., Loukili, A., Grondin, F., 2012, Long term deformations and cracking risk of concrete with high content of mineral additions, *Materials and Structures, 45(11),* 1705-1716.

Briffaut, M., Benboudjema, F., D'Aloia, L., Bahrami, B., Bonnet, A., 2012, Analysis of cracking due to shrinkage restraint in a concrete tunnel, Strategies for Sustainable Concrete Structure, Aix-en-Provence, France, 8 p.

Hearn, N., 1998, Self-sealing, autogenous healing and continued hydration: What is the difference ?, *Materials and structures*, 31, 563-567.

Ter Heide, N., 2005, Crack healing in hydrating concrete, Master Thesis, Université de Delft, Pays Bas, 128 p.
Argouges, M. 2011, Mécanismes et cinétique de l'autocicatrisation dans des mortiers cimentaires : influence de la refissuration, Douzième édition des journées Scientifiques du Regroupement Francophone pour la Recherche et la Formation sur le Béton (RF)²B, Luxembourg, 13 p.
Qian, S., Zhou, J., de Rooij, M.,R., Schlangen, E., Ye, G., van Breugel, K., 2009, Self-healing behavior of strain hardening cementitious composites incorporating local waste materials, *Cement and Concrete Composites*, No. 31, 613–21.
Van Tittelboom, K., Gruyaert, E., Rahier, H., De Belie, N., 2012, Influence of mix composition on the extent of autogenous crack healing by continued hydration or calcium carbonate formation, *Construction and Building Materials*, No. 37, 349-359.
Jacobsen, S., Marchand, J., Hornain, H., 1995, SEM observations of the microstructure of frost deteriorated and self-healed concretes, *Cement and Concrete Research*, No. 25, 1781-1790.
Granger, S., Loukili, A., Pijaudier-Cabot, G., Chanvillard, G., 2007, Experimental characterization of the self-healing of cracks in an ultra high performance cementitious material: Mechanical tests and acoustic emission analysis, *Cement and Concrete Research*, No. 37, 519-527.
Van Tittelboom, K., De Belie, N., Van Loo, D., Jacobs, P., 2011, Self-healing efficiency of cementitious materials containing tubular capsules filled with healing agent, *Cement and Concrete Composites*, No. 33, 497-505.
Poinard, C., Piotrowska, E., Malecot, Y., Daudeville, L., Landis, E., N., 2012, Compression triaxial behavior of concrete : the role of the mesostructure by analysis of X-ray tomographic images, *European Journal of Environmental and Civil Engineering*, 16 :sup1, 115-136.
Landis, E. N., 2013, Emerging imaging techniques applied to concrete durability, Proceedings of the FraMCoS-8/30GEF Workshop, Toledo, Spain, 8 p.
Popic, A., 2010, Influence des ajouts minéraux, des granulats fins, de la température et du rapport eau/liant sur le développement et le contrôle du retrait endogène des matrices cimentaires, Thèse de doctorat, Université de Sherbrooke, Sherbrooke, Canada, 531 p.
Bentz, D., P., 1995, A three-dimensional cement hydration and microstructure program. I. Hydration rate, heat of hydration and chemical shrinkage, *NISTIR 5756*, National Institute of Standards and Technology, Gaithersburg, USA, 60 p.
Argouges, M., Gagné, R., 2009, Étude des mécanismes et de la cinétique de l'autocicatrisation dans des mortiers cimentaires fissurés, Dixième édition des journées Scientifiques du Regroupement Francophone pour la Recherche et la Formation sur le Béton, Cachan, France, 13 p.
Gagné R., Argouges, M., 2012 A study of the natural self-healing of mortars using air-flow measurements, *Materials & Structures*, No. 45 (11), 1625-1638.
Edvardsen, C., 1999, Water permeability and autogenous healing of cracks in concrete, *ACI Materials Journal*, July-August, No. 96, 448-454.
Darquennes, A., Espion, B., Staquet, S., 2013, How to assess the hydration of slag cement concretes ?, *Construction and Building Materials*, No. 40, 1012-1020.
Schindler, A., K., Folliard, K., J., 2005, Heat of hydration models for cementitious materials, *ACI Materials Journal*, January-February, No. 102, 24-33.
Moranville-Regourd, M., 2004, Cements made from blastfurnace slag, *Lea's chemistry of cement and concrete*, fourth edition, Chp. 11, 637-678.
Taylor, H., F., W., 1997, *Cement Chemistery*, Thoms Telford edition, second edition, 459 p.